Direct time-resolved plasma characterization with broadband terahertz light pulses

Virgilijus Vaičaitis,[1,*] Ona Balachninaitė,[1] Aidas Matijošius,[1] Ihar Babushkin,[2,3,4] and Uwe Morgner[2,4]

[1]*Laser Research Center, Vilnius University, Saulėtekio 10, Vilnius LT-10223, Lithuania*

[2]*Institute of Quantum Optics, Leibniz University Hannover, Welfengarten 1, 30167 Hannover, Germany*

[3]*Max Born Institute, Max-Born-Strasse 2a, Berlin 10117, Germany*

[4]*Cluster of Excellence PhoenixD (Photonics, Optics, and Engineering - Innovation Across Disciplines), Welfengarten 1, 30167 Hannover, Germany*

(Received 1 July 2022; accepted 23 November 2022; published 4 January 2023)

We report here the results of comprehensive plasma characterization and diagnostics by analyzing time-resolved absorption spectra of short ultrabroadband (0.1–50 THz) pulses propagated through the test plasma. Spectral analysis of plasma-induced absorption of such THz pulses provides very direct, *in situ*, high dynamical range, potentially single-shot access to the plasma density, plasma decay time, electron temperature, and ballistic dynamics of the plasma expansion. We have demonstrated a proof-of-principle measurement of plasma created by an intense laser beam. In particular, we showed a reliable measurement of plasma densities from around 10^{16} to 10^{20} cm^{-3}. Apart from the plasma parameters, this method allowed us to reconstruct peak intensity inside the plasma spot and to observe a very early stage of plasma evolution after its excitation.

DOI: 10.1103/PhysRevE.107.015201

I. INTRODUCTION

Plasma applications and its diagnostic methods [1] are of paramount importance in many different scientific and industrial fields ranging from controlled fusion [2] and electron acceleration [3] to material processing [4] and medicine [5]. Plasma diagnostics includes a broad range of methods based on spectroscopic, interferometric, electric, and power measurements [1,6–23], allowing one to "look inside" the plasma and infer the free electron density [6–17,20], temperature [17,18] and, in the case when the plasma is produced by a laser pulse, the laser field intensity inside the plasma [21–23] or plasma decay time [24]. Whereas high density plasma is probed by laser or x-ray radiation [25–28], most useful plasma diagnostic techniques for lower plasma density rely on probing with electromagnetic radiation in the microwave range [1,6,7]. The waves reflected from or transmitted through the plasma are measured, with a big advantage of being contactless and not perturbing the plasma. Existing microwave-based methods are complicated, requiring, among others, phase shift measurements for several distinct frequencies. Estimations of electron density are rather indirect and need a separate calibration.

More recently, progress in generating and detecting coherent radiation in the spectral range denoted earlier as the "THz gap," allowed one to employ THz radiation for plasma diagnostics [8–11,19,29–31]. Yet, the methods experimentally realized up to now are rather indirect [8–10,20], or require complex geometry [11,19]. Among them, there are experimental reports on THz time domain spectroscopy (THz-TDS) [8–10], which uses a large portion of the spectrum simultaneously in the form of wide-bandwidth THz pulses transmitted through [19] or generated directly in a plasma [8–11]. This allows one to obtain much larger portions of information from every particular pulse, potentially promising a single-shot operation. These techniques are utilizing the phase shifts of the waves passed through the plasma and require modeling to fit to the experimental data.

In contrast to the above mentioned experimental techniques, the method we introduce here is based on time-resolved THz spectroscopy (TRTS). The key ingredient is the extremely broadband THz pulses of subcycle temporal duration produced in air by two- or multicolor femtosecond laser pulses [32–37]. Such ultrabroadband intense THz pulses have proved their usefulness in various applications, e.g., giving access to measurement and control of various properties of solids [35,38], carrier-envelope phase estimation of short laser pulses [39], control of matter excitations with strong THz transients [38,40], or measurement of the effective tunneling time delays [41]. Their spectrum can span many octaves from hundreds of GHz up to 100 THz, thus in most cases containing simultaneously regions above and below the plasma frequency.

Since the plasma is opaque at the probe frequencies below the plasma frequency ω_p and almost transparent above it, this suggests a simple diagnostic method: An ultrabroadband THz pulse passes through the plasma under test and its spectrum is measured (see inset of Fig. 1). Note that in the region above ω_p the plasma is not absolutely transparent and reflection and absorption are measurable [25–28]. Yet, there is a sharp transition in the spectrum pointing directly to the plasma frequency and thus giving an access to the plasma density. In this paper we present, to the best of our knowledge, the first experimental realization of this technique. Despite its conceptual simplicity, it provides an extremely powerful tool to look inside the plasma, allowing full, time-resolved characterization of gaseous plasma over a wide range of densities. This method

*Virgilijus.Vaicaitis@ff.vu.lt

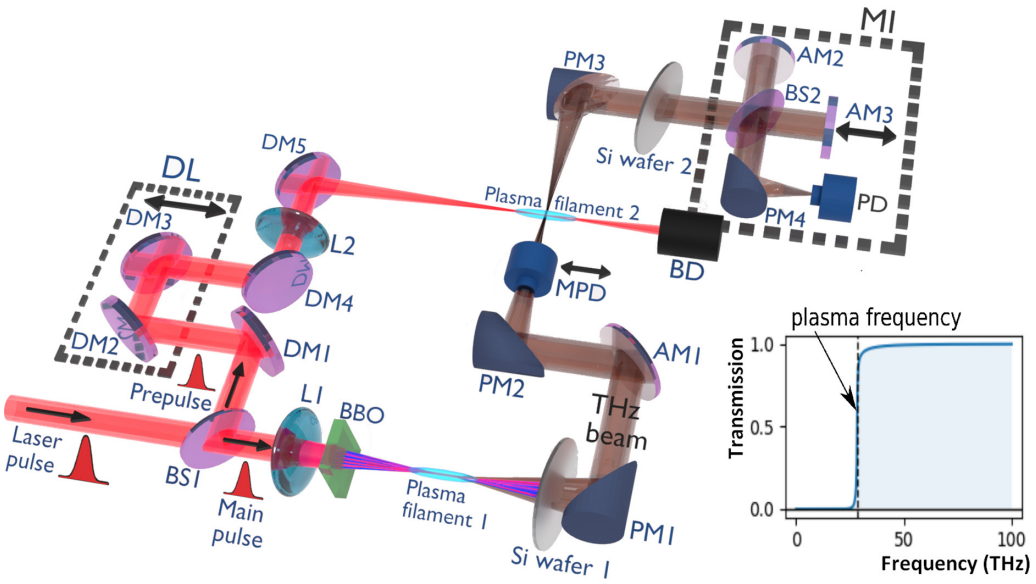

FIG. 1. Experimental setup. The inset shows the general idea of the method: plasma frequency is determined as the position of the abrupt transition from opacity to transparency in the THz spectrum of a pulse transmitted through the plasma. One of the pulses (referred to as the main pulse) is sent to a BBO crystal, where a second harmonic is produced. The THz pulse is generated by the two-color pulses in air (plasma filament 1) and filtered out by a Si plate. The second pulse (referred to as the prepulse) produces the plasma filament 2 after a delay line. The dielectric mirrors DM allow one to vary the position of the plasma filament relative to the THz beam path. BS: beam splitter; L1, L2: lenses with focal lengths of 30 and 10 cm, respectively; PM1, PM2, PM3: parabolic Al coated off-axis mirrors; AM1: flat Al coated mirror; MPD: removable pyroelectric detector; DL: optical delay line; DM: flat dielectric mirror; BD: beam dump; MI: Michelson interferometer.

is compatible with a single-shot operation and allows one to obtain not only the plasma density but also the plasma decay times and, as a consequence, to infer the electron temperature and the peak laser intensity in the case when the plasma is induced by a strong laser pulse. Our method provides an immediate picture of the plasma dynamics in plasma induced filaments, shedding light on the very initial stage of the plasma dynamics e.g. in filaments.

II. RESULTS

In ionized gases, the plasma frequency ω_p is defined as

$$\omega_p = \sqrt{\frac{n_e e^2}{\varepsilon_0 m}}, \tag{1}$$

where n_e is the free electron density and e and m are the electron charge and mass, respectively. Plasma is strongly opaque at the probe frequencies below ω_p and transparent for the frequencies above it (see inset of Fig. 1). More specifically, in the absence of magnetic fields, the propagation k and attenuation α constants for the THz waves in the plasma could be expressed as $k = \mathrm{Re}(\varepsilon^{1/2}\omega/c)$ and $\alpha = -\mathrm{Im}(\varepsilon^{1/2}\omega/c)$, respectively, where ε is the complex dielectric constant given by

$$\varepsilon = \left(1 - \frac{\omega_p^2}{\omega^2 + \nu^2}\right) - i\frac{\nu}{\omega}\left(\frac{\omega_p^2}{\omega^2 + \nu^2}\right). \tag{2}$$

Here ν is the collision frequency, determined by the collision rate of electrons with ions and neutral atoms [18]. By measuring the absorption and its frequency dependence for the electromagnetic waves in plasma, one can deduce the plasma density and the collisional frequency. Moreover, if short electromagnetic pulses are used as a probe, one can even monitor the fast evolution of plasma in time. A somewhat similar technique has already been applied for plasma characterization [8–10]. However, the spectral range of THz-TDS systems used in those experiments was limited to 3–4 THz, therefore so far the information on plasma density had to be deduced from the complex refractive index of the plasma, which requires a careful point-by-point registration and comparison of the original waveform with the transmitted one. The use of broadband THz pulses and registration of the plasma absorption only (as contrasted to the complex refractive index) provides instead a much more precise and robust method, which in addition is fully free of calibration.

To generate THz pulses with spectra spanning the range of 0.1–50 THz we used recently developed techniques which enable covering plasma frequencies $\omega_p = 2\pi f_p$ between $\omega_p = 2\pi \times 0.1$ rad/ps and $\omega_p = 2\pi \times 50$ rad/ps and thereby allow for plasma densities to be studied in a huge range from 1×10^{14} to 3×10^{19} cm^{-3}.

For the experiments we used a 1 kHz repetition rate femtosecond Ti:sapphire chirped pulse amplification laser system (Legend elite duo HE+, Coherent Inc.), delivering 35–40 fs (FWHM) light pulses centered at 790 nm with maximum pulse energies of 8 mJ. The laser pulses were split into the main pulse and the prepulse with energies of 5.2 and 1.65 mJ, respectively. The main pump beam was focused into the ambient air by the lens L1 of about 30 cm focal length through a nonlinear β-phase barium borate (BBO) crystal of 100 μm thickness (type I, cut angles $\theta \approx 29^\circ$ and $\phi \approx 90^\circ$, Fig. 1). Therefore, the main pump beam consisted of overlapping phase locked fundamental and second harmonic (FH, SH)

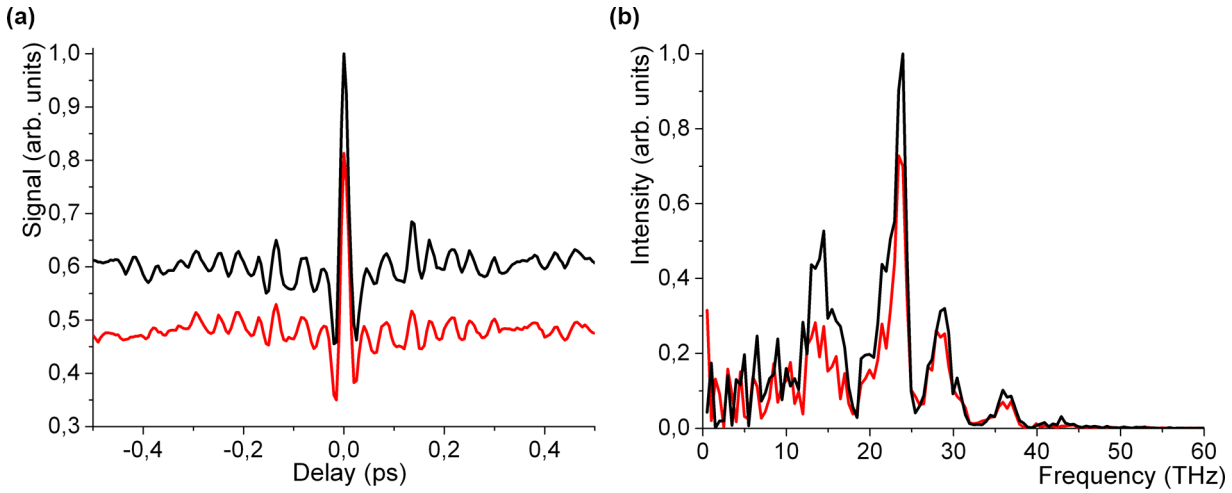

FIG. 2. Typical interference traces (a) and corresponding spectra (b) of the free propagated THz radiation (black curves), and the one transmitted through the plasma (red curves). Energies of the main pulse and prepulse were 5.2 and 1.65 mJ, respectively. Modulation of the spectra is caused by the absorption of used Si filters (the spectral dips almost exactly correspond to the absorption maxima of the float zone Si wafers).

pulses which created the ultrabroadband THz pulses in the plasma filament 1. The azimuthal angle of BBO crystal and its location were optimized to achieve a maximal THz radiation yield [34,42]. Behind the plasma filament 1, a THz filter (0.5–1 mm thick Si wafer 1) was placed to remove the driving pulses from THz beam. The THz pulse was collimated and focused by the aluminum coated off-axis parabolic mirrors PM1, PM2, PM3. The flat mirror AM1 was used for the alignment of collimated THz beam. Energy of the THz pulses was measured using a removable calibrated pyroelectric detector MPD).

The prepulse was focused in the direction orthogonal to the THz beam and generated the plasma filament 2 (Fig. 1). The relative time delay and position of the two interacting pulses were controlled by motorized translation stages and an optical delay line DL. The spatial step was about 0.75 μm, corresponding to temporal delay of 5 fs, and the total scan length was 2 ps (400 measurement points for a single scan).

For measuring the spectra of the THz wave, a home-built Michelson type Fourier spectrometer MI with a THz power detector at the output and a 2 μm thick nitrocellulose pellicle beam splitter were used. By moving the flat mirror in one arm and measuring power on the detector, we were able to register the interferometric traces. The THz spectra were obtained by the Fourier transform. Before the entrance of the interferometer, a second THz filter (Si wafer 2) was placed to remove the residual stray light. Typical measurements and corresponding spectra obtained after averaging over ten interference traces are presented in Fig. 2. Significant spectral amplitude could be observed up to 60 THz.

Overall, the THz signal decreases by interaction with the plasma filament [43–45]. As expected, the transmission is clearly frequency dependent [Fig. 2(b)] and varies with the delay between the pump and the prepulse: The THz signal did not change when the prepulse was sent after the main pulse, but this was not the case when the prepulse created the plasma filament before the main pulse. In this case, after the initial drop, the THz signal slowly recovered with a time constant of about 100 ps, which corresponds well to the ballistic plasma expansion and free electron decay rates reported previously [43,44], as seen in Fig. 3(a).

A more detailed analysis was performed by calculating a normalized THz spectral intensity difference $\Delta = (I_{\text{out}} - I_{\text{in}})/(I_{\text{out}} + I_{\text{in}})$, where I_{in} and I_{out} correspond to the THz spectral intensities of the input and after transmission through the plasma. The average over just a few measurements showed the precise location of the plasma frequency [see Fig. 3(b)] giving, using Eq. (1), the direct access to the plasma density. As the delay between the main laser pulse and the prepulse was increased, we were able to register the decay of the plasma density [see Figs. 3(b) and 4(a)] with the decay time of about 33 ps (corresponding to the two times lower decay rate of the plasma frequency).

To compare our model [defined by Eqs. (1) and (2)] with experiment, we defined the relation of the output intensity I_{out} to the input one I_{in} as $I_{\text{out}} = I_{\text{in}}(f_o + e^{-2\alpha l})/(1 + f_o)$. This expression takes into account the exponential intensity decay with the rate 2α in the plasma of the size l (here we take $l = 1$ mm, but its exact value does not play any important role in the resulting curve). An overlap factor f_o takes into account that not all the light passes through the plasma spot, including also possible additional loss channels due to other dissipation mechanisms. f_o varies from zero (all light comes from the plasma spot and there is no additional loss mechanisms present) to infinity (the losses due to plasma are fully insignificant because neglectingly small part of radiation comes through the plasma).

Using so-defined I_{out} we can calculate Δ in the same way as in experiment and fit the theoretical model to experiment; see Fig. 3(a). We obtained $f_o = 1.15$ as the best fit to the losses below the plasma frequency indicating that the actions of all alternative mechanisms are approximately as strong as the losses due to plasma. The best-fit values of ν and n_e are discussed below. Note that the fits leading to the specific values of n_e, ν, and f_o are obtained from different parts of the experimental curve: n_e was read directly from the position

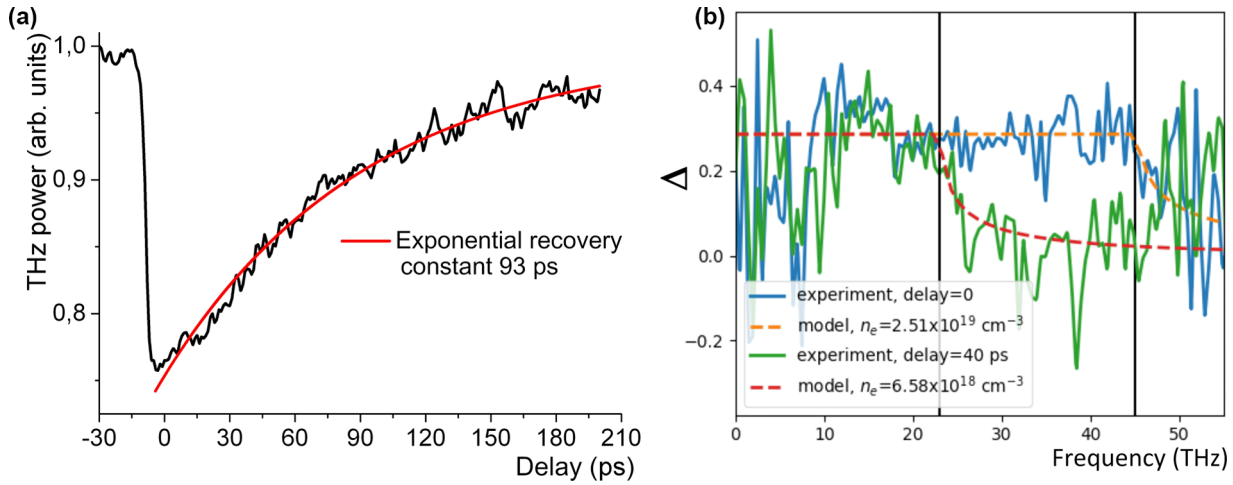

FIG. 3. Measurements of time-dependent frequency resolved THz power. (a) Transmitted THz power (black line) as a function of the delay between the main laser pulse and the prepulse creating the test plasma filament. The red line shows the exponential fit to the decaying tail. (b) Normalized THz spectral intensity difference Δ measured for zero (green line) and 40 ps (blue line) delays between the main pulse and the pre-pulse. Both lines are the averages of ten measurements. Black vertical lines indicate the positions of the plasma frequencies for both cases. Orange and red dashed lines show the values of Δ fitted by the Drude model with the decay constant $\nu = 2$ ps^{-1} and n_e given in the legend.

of the transition in spectrum, ν was determined from the behavior of the experimental curve just above the transition and, finally, f_o was obtained using the part of the curve below the transition point. That is, all of these values are independent of each other, despite being obtained from the same experimental curves, making the fitting procedure especially stable and robust.

We note that the decay time in Fig. 4(a) obtained from the delay-dependent spectra [Fig. 3(b)] is significantly different from the recovery time of the THz power shown in Fig. 3(a), by a factor of about 3. This is because the transmitted THz power [Fig. 3(a)] depends not only on the plasma density, but also on the size of the plasma spot, which changes due to the ballistic plasma expansion. Because of this, the effective volume of the plasma spot is increased, which additionally slows down the THz power recovery. In terms of the input-output relation defined above, not only the plasma density but also the factor f_o changes with time. In particular, the linear geometry of a filament imposes scaling of the electron density as $n_e \sim 1/r^2$, where r is the size of the expanding plasma channel. The attenuation of the THz power is roughly proportional to the product of the plasma density n_e and the interaction length $\sim 2r$. Therefore, the THz power [Fig. 3(a)] scales as $1/r$, much slower than the plasma density $n_e \sim 1/r^2$. This also shows that our method is insensitive to the plasma dimensions and can be applied for the spatially diffused plasmas.

Note that the maximal measured plasma density of 2.5×10^{19}cm^{-3} corresponds to all air molecules being single ionized by the pump pulse. This number provides an excellent independent validity check of our method. On the other hand, the smallest registered plasma density was less than 10^{16} cm^{-3}

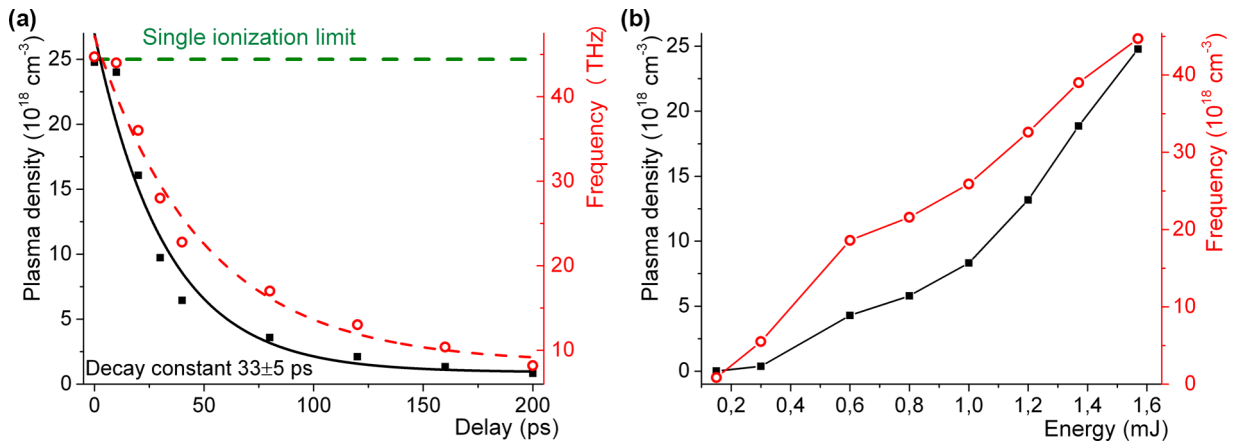

FIG. 4. Time and energy dependence of the plasma density. (a) Experimentally measured plasma frequency (red points and curve) and density (black points and curve) as a function of the delay between the main pulse and prepulse. Note that the decay time of the density is two times larger than that of the frequency. (b) Experimentally measured plasma frequency (black squares) and density (red circles) as a function of the prepulse energy.

[see Fig. 4(b)], demonstrating very large dynamical range of our method (more than 2500). Furthermore, a slope of the drop of Δ with ω for $\omega > \omega_p$ gives us immediately the value of the collision frequency ν as given by Eq. (2). This gives us $\nu \approx 2\text{ps}^{-1}$ for both cases shown in Fig. 3(b).

We note furthermore that this decay is directly related to the collision rate and thus to the electron temperature. To determine the electron temperature based on the collision frequency we use an approach developed in [18]. The collision rate is determined as $\nu = \nu_i + \nu_n$, where ν_i is the decay due to electron-ion collisions and ν_n is the impact from electron-neutral collisions. The former is determined as $\nu_i = n_e c_i T^{-3/2} \ln\Lambda$, where $c_i = e^4/(6\varepsilon_0{}^2\sqrt{2\pi^3 m k_B{}^3})$, k_B is the Boltzmann constant, $\ln\Lambda \approx 4$ is the Coulomb logarithm, $\nu_n = (n_n - n_e)\sigma_e\sqrt{k_B T_e/m}$, $n_n \approx 2.5 \times 10^{19}$ cm^{-3} is the neutral atom density in the absence of excitation, and $\sigma_n \approx 1 \times 10^{-19}$ cm^{-2} is the collision cross section. Using the value of ν retrieved from experiment we immediately obtain the electron temperature T_e, which for zero delay is $T_e \approx 1.5 \times 10^6$ K, whereas for 40 fs delay it decreases to $T_e \approx 800$ K.

We also note that using the electron temperature allows us to infer the peak intensity in the plasma spot. Indeed, as soon as T_e is much larger than the room temperature, the energy obtained by the electrons comes almost entirely from the laser field as a result of energy dissipation. That is, the thermal energy must be approximately equal to the ponderomotive energy of the ionized electrons $U_p = e^2E_p^2/(4m\omega_p^2)$, where E_p is the peak electric field of the pump in the plasma spot, connected to the peak intensity as $I_p = (cn\varepsilon_0/2)E_p^2$. On the other hand, the electron temperature is related to the kinetic energy as $U_p = 3k_BT_e/2$. Equalizing these two expressions for U_p we obtain, that peak temperature mentioned above corresponds to the peak intensity around 3.3×10^{15} W/cm^2.

Both the electron temperature and the peak intensity are noticeably higher than measured before under similar experimental conditions (see, for example, [16]), which we explain by the superior response time of our method in comparison to the fluorescence-based method used in [16].

In a similar way we have registered the dependence of the plasma frequency and density as a function of the prepulse energy. The results are presented in Fig. 4(b). One can see that for the energies of up to 1.6 mJ both of these plasma parameters scale almost linearly and no saturation is observed. This qualitatively corresponds to the previous reports [16], indicating that the linear plasma density scaling takes place also for the laser pulse powers exceeding the critical one. Note that at each prepulse energy point in Fig. 4(b) the plasma density was inferred from its frequency according to Eq. (1). However, the quadratic or square-root dependencies here are not seen since both parameters are also nonlinearly dependent on the prepulse energy.

III. DISCUSSION AND CONCLUSIONS

In conclusion, we have performed a proof-of-principle experiment, demonstrating that the broadband THz pulses can be used to measure plasma frequency, its density, collision frequency as well as the electron temperature with a good temporal resolution. Although here we needed several measurements to obtain the spectra, increasing sensitivity of THz detectors will allow for the single-shot diagnostic in the future. We applied our method to a laser-induced plasma. Our results indicate that even moderately focused femtosecond laser pulses of moderate energy can ionize significant part of the molecules in air. Our data allow us to obtain the plasma collision rate $\nu \approx 2$ ps^{-1}, leading us to estimation of the electron temperatures to be of the order of 10^6 K and therefore to the peak intensities of $\approx$3000 TW/cm^2. The method allows also to track the plasma density dynamically. In our measurements, we obtained the electron density decay time of around 30 ps. Our method is very direct and simple and has a dramatically large dynamical range, making it extremely attractive both in the industry and scientific research, including characterization and monitoring of plasma in tokamaks, wakefield accelerators, and radiation sources based on laser-plasma interactions. As soon as we are limited by the THz range, the plasma densities in the range 10^{16} to 10^{20} cm^{-3} are accessible. But of course, the method can be extended to other frequency regions to grasp even more dense or more dilute plasmas as soon as spectrometry in the corresponding regions is accessible.

ACKNOWLEDGMENTS

V.V. and O.B. acknowledge the Research Council of Lithuania for funding this research by the Grant No. S-MIP-19-46. I.B. and U.M. thank Deutsche Forschungsgemeinschaft (DFG, German Research Foundation), Projects No. BA 4156/4-2 and No. MO 850-20/1, as well as Germany's Excellence Strategy within the Cluster of Excellence EXC 2122 PhoenixD (Project ID No. 390833453) for support.

[1] I. Hutchinson, *Principles of Plasma Diagnostics*, 2nd ed. (Cambridge University Press, Cambridge, 2002).

[2] M. A. Barbarino, Brief history of nuclear fusion, Nat. Phys. **16**, 890 (2020).

[3] A. Modena, Z. Najmudin, A. Dangor *et al.*, Electron acceleration from the breaking of relativistic plasma waves, Nature (London) **377**, 606 (1995).

[4] F. F. Chen, Industrial applications of low-temperature plasma physics, Phys. Plasmas **2**, 2164 (1995).

[5] D. B. Graves, Low temperature plasma biomedicine: A tutorial review, Phys. Plasmas **21**, 080901 (2014).

[6] M. A. Heald and C. B. Wharton, *Plasma Diagnostics With Microwaves* (Wiley, New York, 1965).

[7] Zh. Chen and A. Nikiforov, *Atmospheric Pressure Plasma - from Diagnostics to Applications* (IntechOpen, London, 2019).

[8] S. P. Jamison, J. Shen, D. R. Jones, R. C. Isaac, B. Ersfeld, and D. A. Jaroszynski, Plasma characterization with terahertz time-domain measurements, J. Appl. Phys. **93**, 4334 (2003).

[9] B. H. Kolner, P. M. Conklin, R. A. Buckles, N. K. Fontaine, and R. P. Scott, Time-resolved pulsed-plasma characterization using broadband terahertz pulses correlated with fluorescence imaging, Appl. Phys. Lett. **87**, 151501 (2005).

[10] B. H. Kolner, R. A. Buckles, P. M. Conklin, and R. P. Scott, Plasma characterization with terahertz pulses, IEEE J. Sel. Top. Quantum Electron. **14**, 505 (2008).

[11] A. Curcio and M. Petrarca, Diagnosing plasmas with wideband terahertz pulses, Opt. Lett. **44**, 1011 (2019).

[12] Y. H. Chen, S. Varma, T. M. Antonsen, and H. M. Milchberg, Direct Measurement of the Electron Density of Extended Femtosecond Laser Pulse-Induced Filaments, Phys. Rev. Lett. **105**, 215005 (2010).

[13] S. Eisenmann, A. Pukhov, and A. Zigler, Fine Structure of a Laser-Plasma Filament in Air, Phys. Rev. Lett. **98**, 155002 (2007).

[14] S. Tzortzakis, B. Prade, M. Franco, and A. Mysyrowicz, Time-evolution of the plasma channel at the trail of a self-guided IR femtosecond laser pulse in air, Opt. Commun. **181**, 123 (2000).

[15] D. G. Papazoglou and S. Tzortzakis, In-line holography for the characterization of ultrafast laser filamentation in transparent media, Appl Phys. Lett. **93**, 041120 (2008).

[16] F. Théberge, W. Liu, P. T. Simard, A. Becker, and S. L. Chin, Plasma density inside a femtosecond laser filament in air: Strong dependence on external focusing, Phys. Rev. E **74**, 036406 (2006).

[17] O. Balachninaitė, J. Skruibis, A. Matijošius, and V. Vaičaitis, Temporal and spatial properties of plasma induced by infrared femtosecond laser pulses in air, Plasma Sources Sci. Technol. **31**, 045001 (2022).

[18] Z. Sun, J. Chen, and W. Rudolph, Determination of the transient electron temperature in a femtosecond-laser-induced air plasma filament, Phys. Rev. E **83**, 046408 (2011).

[19] T. J. Wang, J. Ju, Y. Wei, R. Li, Z. Xu, and S. L. Chin, Longitudinally resolved measurement of plasma density along femtosecond laser filament via terahertz spectroscopy, Appl. Phys. Lett. **105**, 051101 (2014).

[20] K. Kang, D. Jang, and H. Suk, Plasma density measurements using THz pulses from laser-plasmas, J. Instrum. **12**, C11003 (2017).

[21] C. Smeenk, J. Z. Salvail, L. Arissian, P. B. Corkum, C. T. Hebeisen, and A. Staudte, Precise in-situ measurement of laser pulse intensity using strong field ionization, Opt. Express **19**, 9336 (2011).

[22] J. Tan, Y. Zhou, M. Li, M. He, Y. Liu, and P. Lu, Accurate measurement of laser intensity using photoelectron interference in strong-field tunneling ionization, Opt. Express **26**, 20063 (2018).

[23] S. Xu *et al.*, Simple method of measuring laser peak intensity inside femtosecond laser filament in air, Opt. Express **20**, 299 (2012).

[24] Ch. Jusko, A. Sridhar, E. Appi, L. Shi, U. Morgner, and M. Kovacev, Filamentation-assisted plasma lifetime measurements in atomic and molecular gases via third-harmonic enhancement, J. Opt. Soc. Am. B **36**, 3505 (2019).

[25] G. Winhart, K. Eidmann, C. A. Iglesias, A. Bar-Shalom, E. Minguez, A. Rickert, and S. J. Rose, XUV opacity measurements and comparison with models, J. Quant. Spectrosc. Radiat. Transfer **54**, 437 (1995).

[26] P. T. Springer, K. L. Wong, C. A. Iglesias, J. H. Hammer, J. L. Porter, A. Toor, W. H. Goldstein, B. G. Wilson, F. J. Rogers, C. Deeney, D. S. Dearborn, C. Bruns, J. Emig, and R. E. Stewart, Laboratory measurement of opacity for stellar envelopes, J. Quant. Spectrosc. Radiat. Transfer **58**, 927 (1997).

[27] T. S. Perry, R. F. Heeter, Y. P. Opachich, P. W. Ross, J. L. Kline, K. A. Flippo, M. E. Sherrill, E. S. Dodd, B. G. DeVolder, T. Cardenas, T. N. Archuleta, R. S. Craxton, R. Zhang, P. W. McKenty, E. M. Garcia, E. J. Huffman, J. A. King, M. F. Ahmed, J. A. Emig, S. L Ayers, M. A. Barrios *et al.*, Replicating the Z iron opacity experiments on the NIF, High Energ. Dens. Phys. **23**, 223 (2017).

[28] T. Nagayama, J. E. Bailey, G. P. Loisel, G. S. Dunham, G. A. Rochau, C. Blancard, J. Colgan, Ph. Cossé, G. Faussurier, C. J. Fontes, F. Gilleron, S. B. Hansen, C. A. Iglesias, I. E. Golovkin, D. P. Kilcrease, J. J. MacFarlane, R. C. Mancini, R. M. More, C. Orban, J.-C. Pain, M. E. Sherrill *et al.*, Systematic Study of *L*-Shell Opacity at Stellar Interior Temperatures, Phys. Rev. Lett. **122**, 235001 (2019).

[29] K. Y. Kim, B. Yellampalle, J. H. Glownia, A. J. Taylor, and G. Rodriguez, Measurements of Terahertz Electrical Conductivity of Intense Laser-Heated Dense Aluminum Plasmas, Phys. Rev. Lett. **100**, 135002 (2008).

[30] S. M. Teo, B. K. Ofori-Okai, C. A. Werley, and K. A. Nelson, Single-shot THz detection techniques optimized for multidimensional THz spectroscopy, Rev. Sci. Instrum. **86**, 051301 (2015).

[31] B. K. Ofori-Okai, A. Descamps, J. Lu, L. E. Seipp, A. Weinmann, S. H. Glenzer, and Z. Chen, Toward quasi-DC conductivity of warm dense matter measured by single-shot terahertz spectroscopy, Rev. Sci. Instrum. **89**, 10D109 (2018).

[32] D. J. Cook and R. M. Hochstrasser, Intense terahertz pulses by four-wave rectification in air, Opt. Lett. **25**, 1210 (2000).

[33] M. Ivanov, I. Thiele, L. Bergé, S. Skupin, D. Buožius, and V. Vaičaitis, Intensity modulated terahertz vortex wave generation in air plasma by two-color femtosecond laser pulses, Opt. Lett. **44**, 3889 (2019).

[34] K. Y. Kim, A. J. Taylor, J. H. Glownia, and G. Rodriguez, Coherent control of terahertz supercontinuum generation in ultrafast laser-gas interactions, Nat. Photonics **2**, 605 (2008).

[35] X. Ch. Zhang, A. Shkurinov, and Y. Zhang, Extreme terahertz science, Nat. Photonics **11**, 16 (2017).

[36] Zh. Zhelin, Ch. Yanping, C. Sen, H. Feng, Ch. Min, Zh. Zhen, Y. Jin, Ch. Liming, Sh. Zhengming, and Zh. Jie, Manipulation of polarizations for broadband terahertz waves emitted from laser plasma filaments, Nat. Photonics **12**, 554 (2018).

[37] V. Vaičaitis, O. Balachninaitė, U. Morgner, and I. Babushkin, Terahertz radiation generation by three-color laser pulses in air filament, J. Appl. Phys. **125**, 173103 (2019).

[38] T. Kampfrath, K. Tanaka, and K. A. Nelson, Resonant and nonresonant control over matter and light by intense terahertz transients, Nat. Photonics **7**, 680 (2013).

[39] M. Kreß, T. Löffler, M. Thomson *et al.*, Determination of the carrier-envelope phase of few-cycle laser pulses with terahertz-emission spectroscopy, Nat. Phys. **2**, 327 (2006).

[40] G. Vampa, T. J. Hammond, M. Taucer *et al.*, Strong-field optoelectronics in solids, Nat. Photonics **12**, 465 (2018).

[41] I. Babushkin *et al.*, All-optical attoclock for imaging tunnelling wavepackets, Nat. Phys. **18**, 417 (2022).

[42] V. Pyragaitė, V. Smilgevičius, K. Steponkevičius, B. Makauskas, and V. Vaičaitis, Phase shifts in terahertz wave generation by tightly focused bichromatic laser pulses, J. Opt. Soc. Am. B **31**, 1430 (2014).

[43] H. Wen, D. Daranciang, and A. M. Lindenberg, High-speed all-optical terahertz polarization switching by a transient plasma phase modulator, Appl. Phys. Lett. **96**, 161103 (2010).

[44] Y. Minami, M. Nakajima, and T. Suemoto, Effect of preformed plasma on terahertz-wave emission from the plasma generated by two-color laser pulses, Phys. Rev. A **83**, 023828 (2011).

[45] V. Vaičaitis, M. Ivanov, K. Adomavičius, Ž. Svirskas, U. Morgner, and I. Babushkin, Influence of laser-preformed plasma on THz wave generation in air by bichromatic laser pulses, Laser Phys. **28**, 095402 (2018).